Elucidating the lotus and rose-petal effects on hierarchical surfaces: Study of the effect of topographical scales on the contact angle hysteresis

Yann Bami Chatenet, Stéphane Valette

Journal of Colloid and Interface Science 676 (2024) 355–367

Contents lists available at ScienceDirect

Journal of Colloid And Interface Science

journal homepage: www.elsevier.com/locate/jcis

Regular Article

Elucidating the lotus and rose-petal effects on hierarchical surfaces: Study of the effect of topographical scales on the contact angle hysteresis

Yann Bami Chatenet *, Stéphane Valette *

Univ Lyon, Ecole Centrale de Lyon, CNRS, ENTPE, Laboratoire de Tribologie et Dynamique des Systèmes, UMR 5513, 69130 Ecully, France

GRAPHICAL ABSTRACT

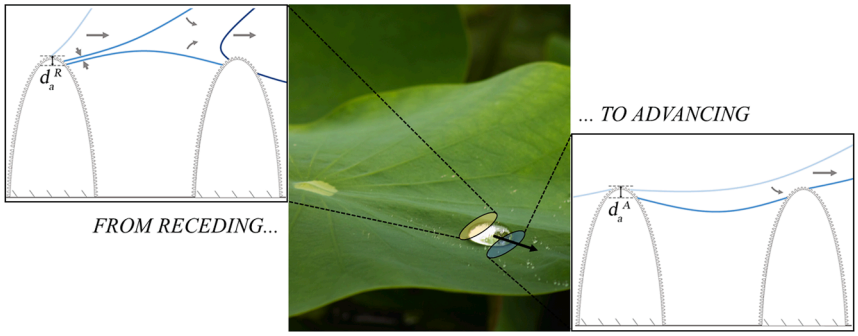

ARTICLE INFO

Keywords:
Adhesion
Cassie-Baxter state
Composite wetting
Multiscale surfaces
Recursion relation
Superhydrophobicity

ABSTRACT

In nature, superhydrophobicity is almost systematically associated with a multiscale topography. Nevertheless, multiscale-textured natural surfaces can either produce water-repellent properties such as on the sacred lotus leaf or high liquid-to-solid adhesion such as on the rose petal. To conceive bio-inspired surfaces with self-cleaning properties, the proper contributions of each topographical scale to the wetting behavior need to be investigated.

Conditions for the equilibrium of menisci produced at a given topographical scale are derived, yielding a recursion relation between each topographical scale. We introduce the equilibrium anchorage depth to quantify the penetration of water at equilibrium. To study the contact angle hysteresis (CAH), we thoroughly describe the mechanisms driving the advancing and receding motions of the triple line. Both phenomena depend on what we define as precursor advancing and receding motions. Eventually, the equilibrium, advancing and receding anchorage depths are related to the CAH.

Topographical heterogeneities at a topographical subscale *i* are always associated with a reduced equilibrium anchorage depth and an enhanced robustness at all topographical scales of higher orders of magnitude. Eventually, it is demonstrated that advancing and receding anchorage depths are bounded by the equilibrium anchorage depth, elucidating how rose-petal-like surfaces systematically produce a high CAH.

* Corresponding authors.
E-mail addresses: yann.bami-chatenet@ec-lyon.fr (Y. Bami Chatenet), stephane.valette@ec-lyon.fr (S. Valette).

https://doi.org/10.1016/j.jcis.2024.07.114
Received 19 March 2024; Received in revised form 9 July 2024; Accepted 13 July 2024
Available online 16 July 2024

Nomenclature

Symbol	Definition *[Unit]*
Latin letters	
b_i	= Half-spacing between consecutive asperities constituting the topographical scale i *[m]*
C_i	= Curvature of a meniscus produced at the topographical scale i *[m^{-1}]*
C_{macro}	= Macroscopic curvature of the liquid droplet *[m^{-1}]*
$d_{a,i}$	= Anchorage depth of menisci at the topographical scale i *[m]*
$d^*_{a,i}$	= Equilibrium anchorage depth of menisci at the topographical scale i *[m]*
$d^A_{a,i}$	= Advancing anchorage depth of the triple line at the topographical scale i *[m]*
$d^m_{a,i}$	= Anchorage depth at the scale i at the location of maximal apparent local slope *[m]*
$d^R_{a,i}$	= Receding anchorage depth of the triple line at the topographical scale i *[m]*
g	= Gravitational acceleration *[$m\cdot s^{-2}$]*
$\overline{h}_i$	= Mean height of asperities constituting the topographical scale i *[m]*
w_i	= Apparent fraction of liquid–vapor interface area at the topographical scale i
$z_{c,i}$	= Vertical depth between the apex of the meniscus (at the scale i) and its anchor point *[m]*
$z_{f,i}$	= Free height between the apex of the meniscus (at the scale i) and the valley *[m]*
Greek letters	
γ	= Liquid-vapor interfacial tension *[$N\cdot m^{-1}$]*
ΔP_i	= Pressure gradient above a meniscus (at the scale i) *[Pa]*
$\Delta p_{Laplace}$	= Laplace pressure of a curved liquid–vapor interface *[Pa]*
$\Delta P_{max,i}$	= Maximal overpressure sustainable by a meniscus at the scale i before transiting *[Pa]*
Δz	= Height of the top of the liquid droplet *[m]*
$\Delta\theta_i$	= Contact angle hysteresis (CAH) at the scale i, equals $\theta_{A,i}-\theta_{R,i}$ *[°]*
$\theta_{A,0}$	= Intrinsic advancing contact angle *[°]*
$\theta_{A,i}$	= Apparent advancing contact angle at the topographical scale i *[°]*
$\theta_{R,i}$	= Apparent receding contact angle at the topographical scale i *[°]*
θ_i	= Equilibrium contact angle (ECA) at the topographical scale i *[°]*
λ_i	= Apparent external-triple-line linear density at the topographical scale i
ρ	= Density of the liquid
ω_i	= Apparent local slope of an asperity sidewall at the topographical scale i *[°]*
ω_i^{max}	= Maximal apparent local slope at the topographical scale i *[°]*
$\omega_{sc,i}$	= Threshold value of ω_i for which $\Delta P_i = 0$ *[°]*

1. Introduction

The discovery of natural surfaces displaying outstanding wetting behaviors has sparked the interest of researchers on how water – among other liquids – interacts with textured surfaces. Since Barthlott and Neinhuis shed light on the link between the self-cleaning abilities of the superhydrophobic lotus leaf and its surface topography [1], theoretical advances have led to a better understanding of how a hierarchical surface topography could be a major asset for repelling liquids in an efficient and robust manner [2–6]. From the model introduced by Cassie and Baxter, relative to the composite-wetting of a textured surface and the entrapment of air bubbles beneath menisci [7], Herminghaus formally demonstrated how hierarchical surfaces produced high equilibrium contact angles (ECAs) due to the effect of each topographical scale on the geometrical equilibrium occurring at the scales of larger sizes [2]. He consequently introduced a recursion relation for the cosine of the ECA:

$$\cos(\theta_{n+1}) = (1-w_n)\cos\theta_n - w_n \quad (1)$$

where θ_n is the ECA at the scale n, that is, the ECA that would be measured on a surface constituted of all topographical scales from $i=0$ to n, and w_n is, in Herminghaus' notation, the apparent fraction of liquid–vapor interface area, essentially due to the suspension of the meniscus at the scale n. The reader should note that, here and for the rest of the article as well, a larger n is related to a larger length scale. Eq. (1) demonstrates how hierarchical surfaces are associated with larger ECAs, and, therefore, dramatically enhance hydrophobicity. However, hydrophobicity does not mean low adhesion, even though large ECAs have been considered to be an important condition for water-repellency since they generally lead to low roll-off angles [6,8]. As within Herminghaus' work, a lot of efforts have been directed towards predicting the macroscopic ECA from the chemical and topographical characterization of a given surface.

Nevertheless, the ECA is insufficient to describe the way a surface interacts with a liquid drop. More particularly, the liquid-substrate adhesion cannot be measured on real surfaces through the sole value of the ECA. Indeed, despite the Young-Dupré equation yielding the solid–liquid work of adhesion from the value of the ECA, Pease claimed, as early as 1945 [9], that the existence of a certain range of admissible contact angles (namely, the contact angle hysteresis (CAH)) made it impossible to determine the mean work of adhesion through the measure of the ECA. To quote from his work [9]: 'This line of junction [the triple line, at the interface between the solid, liquid and vapor phases] can occupy various possible parallel positions on the plane of the solid surface, and different positions allow different mean works of adhesion depending upon the configuration of the different groups exposed on the solid surface'. Considering the ECA to measure the liquid-substrate adhesion would come to ignoring the existence of a range of admissible works of adhesion. Therefore, several authors have attempted to draw a link between the liquid-substrate adhesion and the contact angle hysteresis, assuming that the macroscopic adhesion of a drop to a substrate can be indirectly quantified by the measure of the contact angle hysteresis (CAH) displayed by the system [8,10–11]. The CAH is defined as the difference between the advancing contact angle – the contact angle measured at the triple line when the latter starts wetting an unwetted area – and the receding contact angle – measured when the triple line starts dewetting a wetted area. As claimed by Pease, 'the receding contact angle is related directly to the line of greatest possible mean work of adhesion' when 'the advancing contact angle is dependent upon the greatest possible amount of work necessary to wet the solid surface […] [which,] in turn, is inversely related to the least possible mean work of adhesion' [9]. According to Furmidge, and as derived in his work [8], the force of adhesion of the liquid onto the substrate along the triple line is proportional to the amplitude of the CAH. Therefore, the measure of the CAH has been used by many authors to give an undirect image of the liquid-substrate adhesion of a given system [8,10–11]. Other techniques can be employed for this purpose, such as capillary-deflection techniques [12–13] or force-distance measurements

[14–15]. These techniques can help overcoming the difficulties inherent in goniometry measurements, essentially due to the poor precision of the images used, which introduce numerous sources of measurement error. In spite of the latter, goniometry measurements are still widely used to characterize the wetting properties of a surface.

As a consequence, apart from its potential lack of precision, the CAH can be used as a measure of the liquid–solid adhesion, whereas the sole value of the ECA cannot. It is noteworthy that the ECA is not predictive of the CAH, which makes it even more so unsuitable for the study of the adhesion of liquid droplets to solid surfaces. As a matter of fact, Slippery Liquid-Infused Porous Surfaces (SLIPS) exhibit low ECAs while producing low roll-off (or sliding) angles due to an extremely low CAH [16]. On the other hand, surfaces displaying a large ECA but a large CAH have been reported and are often associated with intermediate wetting of surface protrusions [17] or, in the case of multiscale surfaces, water significantly penetrating between micrometric protrusions in spite of the entrapment of air between nanoscale reliefs – a behavior referred to as the "rose-petal effect" [18–19]. Such surfaces do not have self-cleaning properties since droplets of water are pinned onto the surface. Indeed, Furmidge's law [8] predicts that a large CAH is associated with a droplet being unable to undock from the surface even when submitted to an upside-down tilting. As a consequence, the potential of hierarchical surfaces for water-repellency depends on the wetting state occurring at each topographical scale, and, more precisely, on the degree of penetration of water between topographical protrusions.

Quantifying the degree of penetration of water comes to measuring the equilibrium (or effective) anchorage depth of menisci that are suspended between surface asperities, such as depicted in Fig. 1[f]. Unfortunately, only limited attention has been devoted to the study of intermediate wetting and to the prediction of the equilibrium anchorage depth of menisci between surface asperities. The main reason is that many authors have chosen to focus their study on ideally cylindrical asperities, as depicted in Fig. 1[c]. In such a case, either the meniscus is trapped at the discontinuity between the top and the vertical wall, either the air-entrapment fails and water fully penetrates between asperities, which is referred to as a Wenzel state. However, these ideal asperities do not exist in nature, such as schematically depicted in Fig. 1[f] and shown in Fig. 2 for the case of the sacred lotus. On real surfaces, an intermediate wetting can occur: the meniscus can be trapped somewhere along the sidewall of an asperity. Now, that brings us to a very important question:

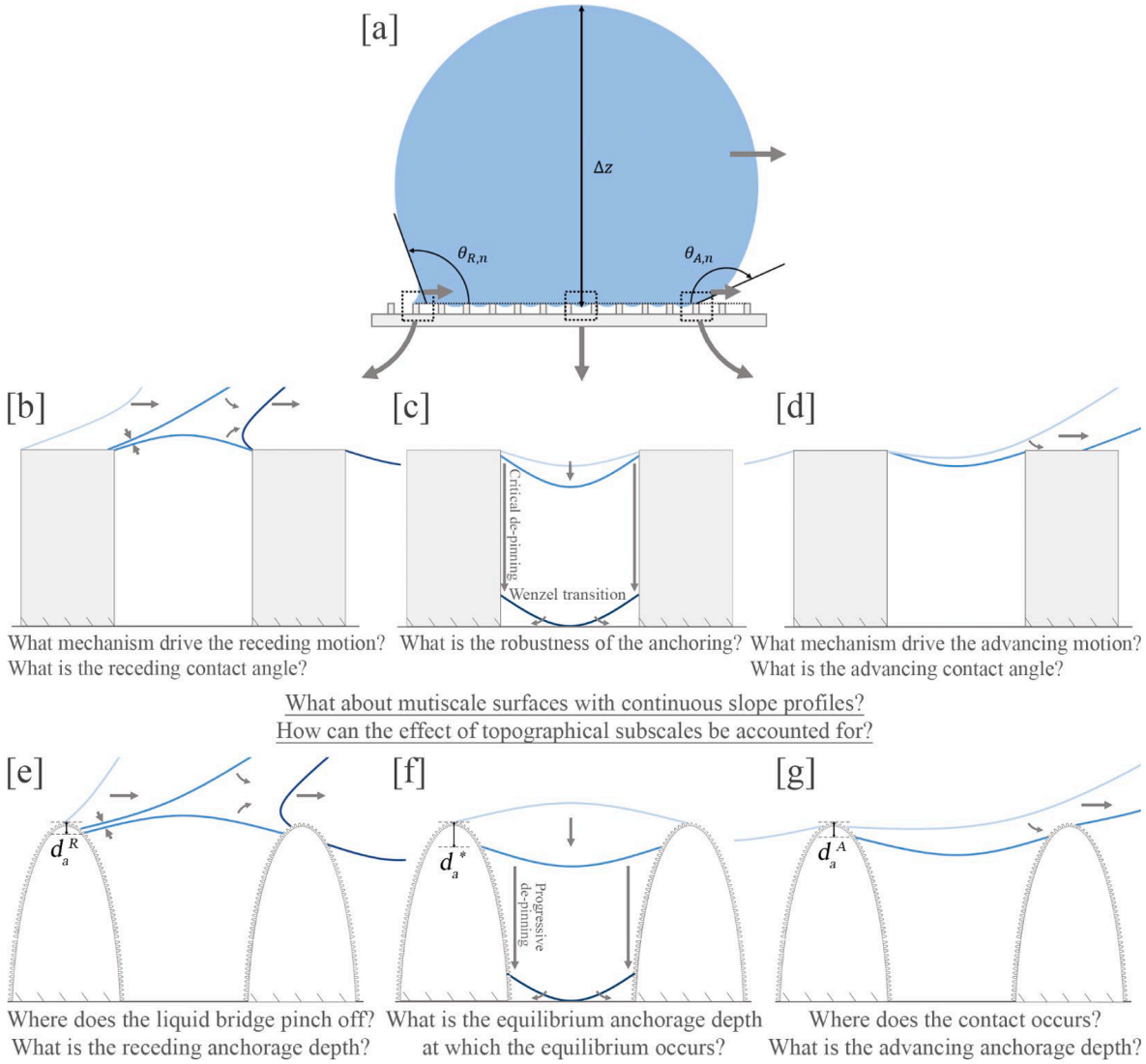

Fig. 1. Schematic representation of a drop deposited onto a textured surface and entering into a lateral motion [a], with close-up views on the equilibrium established beneath the drop in the case of a model surface [c] and a real surface [f], close-up views on the mechanism underlying the receding motion of the drop in the case of a model surface [b] and a real surface [e], and close-up views on the mechanism underlying the advancing motion of the drop in the case of a model surface [d] and a real surface [g]. The multiscale topography of a real surface enhances the complexity of the theoretical study and raises new fundamental questions that must be addressed.

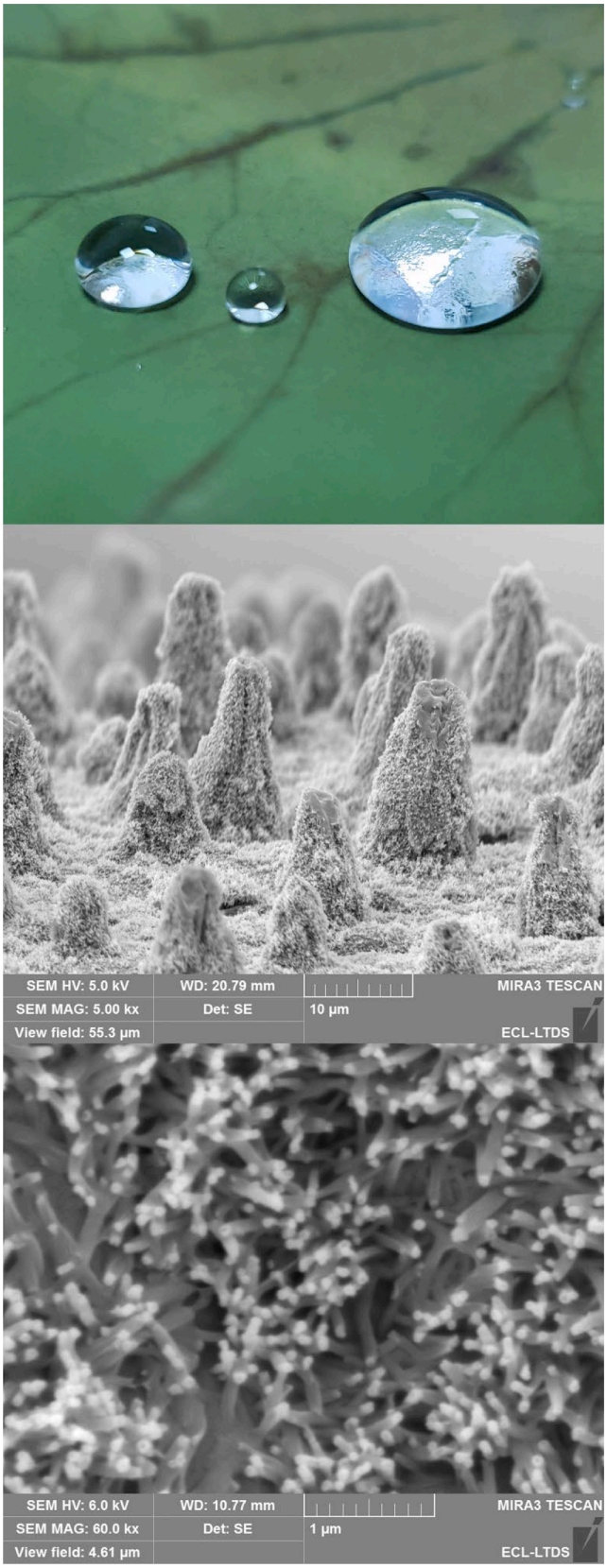

Fig. 2. [from top to bottom] Photography of water droplets resting on a sacred lotus leaf; SEM images of the adaxial side of a *Nelumbo nucifera* (sacred lotus) leaf (x3k and x60k). Leaves were obtained from the botanical garden of Lyon.

when one gently (quasi-statically) puts a droplet of water on a textured surface such as a sacred lotus leaf, where will the triple line stop? Where will the equilibrium be produced along the sidewall of the asperities?

Once again, this question has not received much attention, despite the difference of behavior between a lotus leaf and a rose petal being significantly affected by the degree of penetration of water between micrometric asperities. Water is suspected to fully penetrate between micrometric protrusions on the rose petal [18] while air is trapped at the nanoscale between nanofolds, producing what can be referred to as a Wenzel-Cassie hierarchical wetting state. On the other hand, we have predicted in previous works that the micrometric menisci would be anchored onto cellular papillae of the sacred lotus *(Nelumbo nucifera)* leaves at an equilibrium anchorage depth between 120 and 220 nm [20–21], suspending the bottom of the protruding menisci at a free height of about 12.5 µm above the valleys. These results suggest two things. First of all, when studying the sacred lotus leaf, we have shown that, even on superhydrophobic surfaces, an intermediate wetting state can occur at the micrometric scale since the equilibrium anchorage depth of triple lines is not equal to zero and a portion of the top of micrometric cellular protrusions is actually wet. Second of all, the difference of behavior between the rose petal and the sacred lotus yields the conclusion that the degree of penetration of water between micrometric protrusions is undoubtedly a critical parameter for the macroscopic CAH of a droplet. Therefore, its quantification and its prediction should be investigated. But these surfaces are not like those usually studied in the literature: they display a multiscale topography. This raises a major issue: how can we account for the effect of topographical subscales on the equilibrium of menisci? What impact does a multiscale topography have on the equilibrium and its robustness? We have partially answered to these questions in previous works [20–21], but we wish here to explore these effects more thoroughly and to formalize the equations that help us understand them.

However, studying the equilibrium anchorage depth is not enough: in order to link the penetration of liquid at equilibrium (in other terms, the equilibrium anchorage depth) to the CAH, other questions arise. What are the mechanisms that drive the advancing and receding motions of the triple lines on textured surfaces, in an air-entrapment state? Where, when and how do the triple lines advance to the next row of asperities or recede from the last one? Can we define an advancing anchorage depth and a receding anchorage depth, as depicted in Fig. 1 [e] and 1 [g], and relate these values to the value of the CAH? How do the equilibrium anchorage depth, the slope and other topographical parameters impact these values? How is the effect of the CAH proper to a given topographical subscale propagated to the macroscopic picture? While some theoretical works have addressed these questions on ideally cylindrical surfaces [22–23], the answers are not applicable to surfaces displaying asperities that are neither ideally vertical on their sides nor flat at their tops.

Studying the equilibrium penetration into surface asperities of a droplet comes to studying the transition between different wetting states. The transitions between different wetting states have been the focus of many theoretical works in the past decades [3,5,17,24–31]: but none has, at the same time, considered a non-ideal geometry, a multiscale topography, and the possibility of an intermediate state. Some authors have, nevertheless, studied the penetration of liquid between asperities, but unfortunately, it has always been done on ideal geometries [30,32–34]. Jiang *et al.* derived an analytical modeling of the impregnation of mono-scale textured surfaces from an energetical approach and predicted the equilibrium liquid penetration depth on four types of model topographies [34]. However, applying such an approach to complex natural surfaces like the lotus leaf is inconceivable, since it would be difficult to describe their complex nanoscale topography constituted of randomly-distributed wax crystals of various lengths and widths (as depicted by secondary electron microscopy images in Fig. 2) as well as the complex chemical heterogeneity of the surface at the molecular scale in such an appropriate manner for the energetical

approach to be suitable for a dynamic description of the motion of the triple lines [21]. Furthermore, no study has, to our knowledge, ever tried to draw a quantitative link between the amount of penetration of liquid and the macroscopic CAH.

As emphasized in a previous work, it is possible to model the impregnation of complex surfaces from a critical pressure approach [21]: the latter requires to predict the curvature of the meniscus at every anchorage depth along the sidewalls of a set of two micrometric papillae to which it is suspended. To do so, and as we have previously described, one must know the profile of the apparent instantaneous slope at the micrometric scale as well as the local advancing contact angle formed by the triple line as the latter is descending along the surface of the micrometric protrusions. The latter consideration is of prime importance for the study of transitions [17,22], and previous authors erroneously did not consider the triple line to be at its advancing geometry when modeling the impregnation of surface asperities, instead using Young's intrinsic contact angles [2,32,34].

To conclude this introduction, it must be emphasized that if a lot of efforts have been directed towards the modeling of wetting on textured surfaces, it is, to this day, not yet possible to predict the comprehensive effect of a complex multiscale-textured surface on wettability and solid–liquid adhesion. As a consequence, it remains impossible to precisely quantify the proper effect of an additional topographical scale on the wettability of a surface, and therefore, to predict the benefit of the production of a hierarchical surface through a more complex manufacturing process. Eventually, although the lotus and the rose-petal effects are well-known, they are far from being well understood: to our knowledge, it is not yet possible to quantitatively link the degree of penetration of water between surface protrusions to the CAH. We believe that this knowledge gap takes its source in the fact that the physical mechanisms driving the motion of the contact line have not been fully described yet.

Therefore, in this article, we wish to bring answers to these questions. First of all, we formally demonstrate that, for a surface constituted of $n+1$ independent topographical scales, there is a recursion relation between the advancing contact angle at any scale $i \leq n$ and the equilibrium anchorage depth at the scale $i+1$, and, more practically, that the latter only depends on the profiles of spacing between asperities and instantaneous slope at the scale $i+1$ and on the advancing contact angle at the scale i. For the first time, the mechanisms underlying the advancing and receding motions of the triple line on real surfaces (with a continuous slope profile) are thoroughly described and modeled. The relevance of a given topographical subscale with regards to its effect on the macroscopic CAH and the robustness of the composite-wetting state is discussed to the light of this modeling. Eventually, the link between a larger equilibrium anchorage depth and a larger adhesion is demonstrated, clarifying the physical origin of the rose-petal effect. We believe that these theoretical derivations are a necessary first step towards the prediction of contact angle hysteresis on complex surfaces, a goal which is currently out of range of existing theoretical models.

2. Theory and calculation

2.1. Critical pressure criteria for the prediction of equilibrium anchorage depths on multiscale surfaces

Our first purpose is to derive criteria for the equilibrium of menisci on a mono-scale textured surface: it comes to initializing the recursion relation that will be explored thereafter. We therefore consider a droplet of water deposited on a mono-scale textured surface constituted, for instance, of lotus-like pillars – or papillae – attributed to the scale $n = 1$. The surface of these papillae, *i.e.*, the scale $n-1 = 0$, is considered atomically flat. In a previous work [21], we have introduced equilibrium criteria based on the continuity of pressure across the meniscus, enabling the retrieval of the equilibrium anchorage depth, $d^*_{a,i}$, on the sidewalls of the asperities constituting a given topographical scale i, as depicted in Fig. 3[a] in the case $i = n = 1$. For the equilibrium to be possible, the local curvature of the meniscus, C_i, as illustrated in Fig. 3 [a], must be such that the overpressure between the pressure of the liquid particles along the liquid–vapor interface and the pressure in the vapor phase beneath the meniscus (namely, the overpressure given by Laplace's law applied to the local curvature of the meniscus, $\Delta p_{Laplace,local}$) matches the overpressure in the bulk right above the liquid–vapor interface due to the macroscopic curvature of the drop of water ($\Delta p_{Laplace,macro}$) and to the effect of gravity ($\rho g \Delta z$, where ρ is the

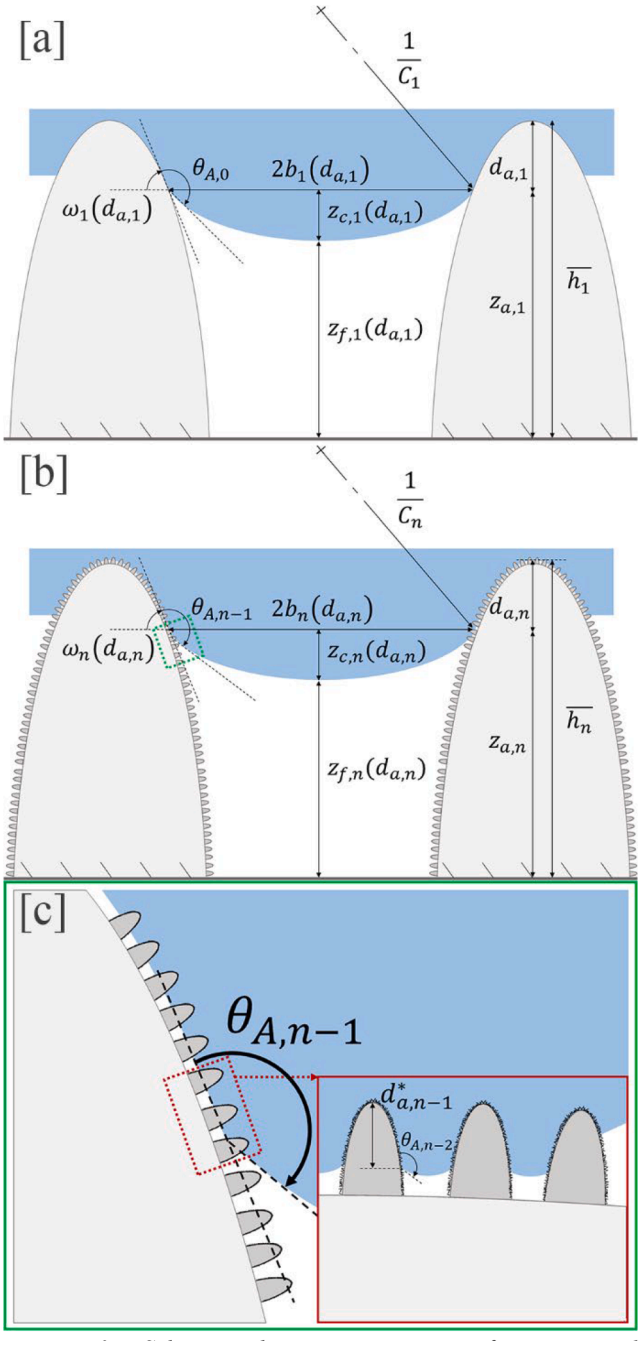

Fig. 3. Schematical representations of geometrical equilibriums produced on a multiscale surface with n topographical scales: [a] at the scale i = 1 [b] at the scale i = n [c] close-up views on the triple lines formed on asperities constituting the topographical scale i = n (in green) and i = n −1 (in red). (For interpretation of the references to colour in this figure legend, the reader is referred to the web version of this article.)

liquid density, g is the acceleration due to gravity and Δz is the depth of the apex of the meniscus with respect to the top of the drop, as illustrated in Fig. 1[a])). In other terms, the pressure gradient between the local liquid–vapor interface and the bulk right above the meniscus, ΔP_i – which is initially negative when the drop is deposited – must vanish. The latter quantity is defined as $\Delta P_i(d_{a,i}) = \Delta p_{Laplace,local} - \Delta p_{Laplace,macro} - \rho g \Delta z$. A second condition is that the bottom of the protruding meniscus shall not enter into contact with the valley. For the latter to be satisfied, the free height, $z_{f,i}(d_{a,i})$, namely, the height between the bottom of the meniscus and the valley – as illustrated in Fig. 3[a], must be strictly positive. In mathematical terms, the equilibrium is produced when the following conditions are verified (with the aim of reasoning across multiple topographical scales, Eqs. (1) to (4) are generalized for any topographical scale i; in the case of the above-mentioned example, one shall consider $i = 1$):

$$\begin{cases} \Delta P_i(d_{a,i}) = \gamma C_i(d_{a,i}) - \gamma C_{macro} - \rho g \Delta z = 0 \\ z_{f,i}(d_{a,i}) = \overline{h}_i - d_{a,i} - z_{c,i}(d_{a,i}) > 0 \end{cases} \quad (1)$$

where γ is the liquid–vapor interfacial tension, C_{macro} is the macroscopic curvature of the liquid drop (which is a trivial function of the volume of the drop and of the macroscopic equilibrium contact angle), $\overline{h}_i$ is the mean height of the asperities constituting the topographical scale i (see Fig. 3[a]),$d_{a,i}$ is the anchorage depth at that scale, and $z_{c,i}(d_{a,i})$ is the vertical amplitude of the protrusion of the meniscus (also referred to as the critical height), as depicted in Fig. 3[a]. Simple geometrical considerations demonstrate that both the local curvature, $C_i(d_{a,i})$ and the critical height, $z_{c,i}(d_{a,i})$, as both depicted in Fig. 3[a], are functions of the half-spacing between two asperities at the current anchorage depth, $b_i(d_{a,i})$ (see Fig. 3[a]), the local slope (namely, the angle between the horizontal and the plane that is locally tangent to the apparent surface at the scale i), $\omega_i(d_{a,i})$ (see Fig. 3[a]), and the local advancing contact angle formed by the triple lines when the latter are descending along the sidewalls of the asperities and which corresponds to the advancing contact angle at the scale $i-1$, $\theta_{A,i-1}$ (in our example, $\theta_{A,0}$):

$$C_i(d_{a,i}) = \frac{-\sin(\omega_i(d_{a,i}) + \theta_{A,i-1})}{b_i(d_{a,i})} \quad (2)$$

and

$$z_{c,i}(d_{a,i}) = b_i(d_{a,i}) \tan\left(\frac{\omega_i(d_{a,i}) + \theta_{A,i-1} - \pi}{2}\right) \quad (3)$$

The equilibrium anchorage depth at the topographical scale i, $d^*_{a,i}$, can be found from the definition given by Eq. (4):

$$d^*_{a,i} = \min\{d_{a,i} | \Delta P_i(d_{a,i}) = 0 \text{ and } z_{f,i}(d_{a,i}) > 0\} \quad (4)$$

Eventually, if $d^*_{a,i} \to 0$, an ideal Cassie-Baxter state is observed at this topographical scale. Conversely, as $d^*_{a,i} \to \overline{h}_i$ or if $d^*_{a,i}$ does not exist, the system tends towards a Wenzel state (again, only at the scale i). The interval of anchorage depths between those two extrema are referred to as a mixed-state wetting or an intermediate wetting. We shall specify that, in spite of the common tendency to represent a Cassie-Baxter state as menisci perfectly anchored to the very top of solid asperities, a mixed-state wetting case was actually used to derive the equations introduced by Cassie and Baxter in their original article published in 1944. To resolve any ambiguity, we herein distinguish an *ideal* Cassie-Baxter state wetting from a mixed-state wetting, as defined hereabove. From a practical point of view, and to get back to our example ($n = 1$), if a mixed-state or a Wenzel wetting is commonly observed, an ideal Cassie-Baxter state is only theoretical, as the latter would require either $\theta_{A,0} = \pi$ or a perfect discontinuity at the edge of a flat-top asperity producing a slope profile such that $\omega_1(0) = 0$ and, for all $d_{a,1} > 0$, $\omega_1(d_{a,1}) > \omega_{sc,1}(d_{a,1})$, where $\omega_{sc,1}(d_{a,1})$ is the minimal value of the local slope for which the sufficient condition on the pressure gradient is verified, that is, the slope for which $\Delta P_1(0)$, the pressure gradient above the meniscus when the latter is anchored to the top edge, vanishes (note that $\omega_{sc,1}(d_{a,1})$ is still a function of the anchorage depth since it is a function of the local spacing between two anchor points, $b_1(d_{a,1})$). Nevertheless, despite photolithography-based manufacturing processes producing quasi-perfect micrometric pillars, no known method can yield sharp edges at the atomic scale. As a consequence, the equilibrium anchorage depth, $d^*_{a,i}$, is never exactly equal to zero.

Now, let a surface be such that it is constituted of the superposition of the previously described topography, associated with the scale $i = n-1 = 1$, and another lotus-like structure at a scale $i = 2$ of greater order of magnitude, very large with respect to the previous one, as depicted in Fig. 3[b] (for $n = 2$). At the very moment the drop of water enters into contact with this surface, triple lines are *apparently* created at the top of asperities constituting the scale $i = 2$. These asperities being covered with asperities of a smaller size ($i = 1$), the triple lines are actually created at the scale $i = 1$, as an equilibrium locally occurs. The latter is characterized by the local impregnation of the smallest asperities until the equilibrium anchorage depth $d^*_{a,1}$ is locally reached. As this local equilibrium is established, the triple line apparently created at the scale $i = 2$ forms a local advancing contact angle, $\theta_{A,1}$ – whose value depends on the topographical parameters related to the scale $i = 1$. The triple line vertically penetrates the interspace between the asperities constituting the scale $i = 2$ until the meniscus formed at this topographical scale reaches a sufficient curvature. Therefore, the impregnation of the scale $i = 2$ is driven by an advancing motion of the triple line at the scale $i = 1$, as the latter propagates through rows of asperities – again, forming an advancing contact angle $\theta_{A,1}$ – thanks to the mechanism that will be described later on.

The impregnation of the topographical scale $i = 2$ is only governed by the profiles $b_2(d_{a,2})$ and $\omega_2(d_{a,2})$ and by the advancing contact angle produced at the scale $i = 1$, since Eq. (2) demonstrates, when applied to $i = 2$, that these parameters entirely define the curvature of the meniscus, yielding, by Eqs. (1) to (4), the derivation of the equilibrium anchorage depth at the topographical scale $i = 2$, $d^*_{a,2}$. By immediate recursion, the same considerations are applicable to any topographical scale constitutive of a multiscale surface formed by n topographical scales, as depicted in Fig. 3[b] and 3[c] and as further discussed in the part 'Discussion'.

2.2. On the mechanism of the advancing motion of triple lines on a multiscale surface

The knowledge of the equilibrium anchorage depth is a first step towards predicting the macroscopic CAH. To understand the difference between the wetting behavior of the lotus leaf and that of the rose petal, we wish to clarify the mechanisms that drive the advancing and receding motions of triple lines on multiscale surfaces. Both the apparent advancing and receding contact angles at a given topographical scale i, $\theta_{A,i}$ and $\theta_{R,i}$, are functions of the contact line density. It has indeed been claimed by previous authors [18,22,26] that the contact angle produced in a composite-wetting state on a textured surface is given by a mixture distribution of the local advancing or receding contact angle formed at the solid–liquid interface and of the angle formed at the liquid–vapor interface (the latter being equal to π), weighted by the external-contact-line linear density, $\lambda_i(d_{a,i})$ (the quantity expressed by Extrand as λ_p [22]). That being said, the local advancing and receding contact angles formed at the solid–liquid interface are given by different mechanisms that have been only slightly described in the literature and which shall, therefore, be investigated in order to determine the parameters that exert an effect on the values of said angles.

Fig. 4[a] depicts a triple line submitted to an advancing motion on a multiscale surface constituted of n topographical scales displaying a composite-wetting state at the scale n. For the sake of the discussion, we

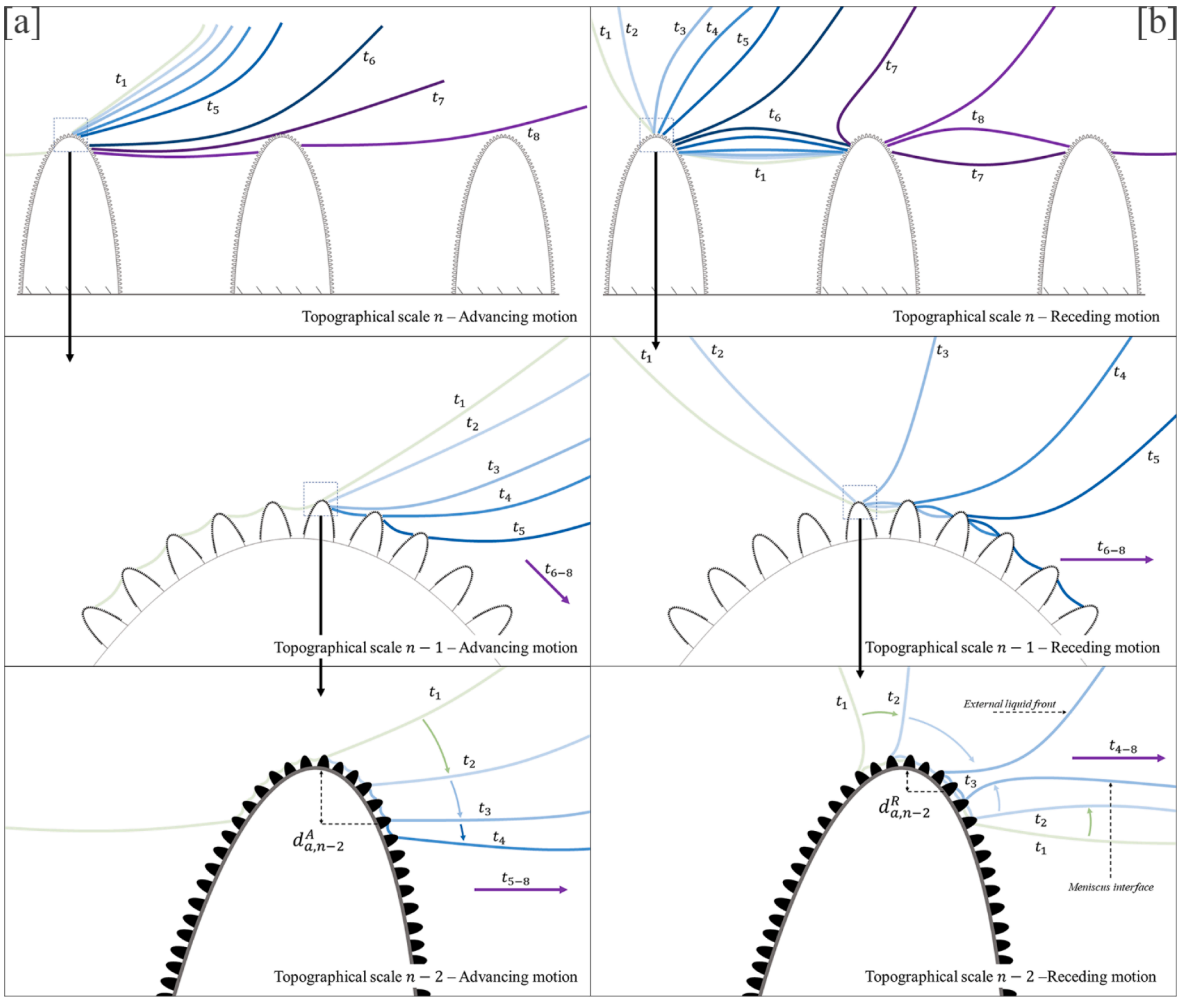

Fig. 4. Schematical description of the mechanisms underlying the advancing ([a]) and receding ([b]) motions of the triple lines on real multiscale surfaces: [a] The advancing motion requires the liquid–vapor interface to enter into contact with the neighboring asperity, which can only occur if precursor advancing motions unfold at all topographical subscales; [b] The receding motion occurs when the triple line pinches off and ruptures, which requires two phenomena of precursor receding motions to unfold at all topographical subscales, one at the location of the external triple line and one at the location of the anchorage of the meniscus. As the triple line pinches off and recedes, a perturbation wave propagates through the liquid–vapor interface (see [b] t_7 at scale n).

consider this motion to be caused by an increase of the volume of the droplet, after that an equilibrium had initially occurred. For the composite-wetting state to be maintained as the triple line advances towards the next row of asperities, the motion of the latter can only result from the contact between an upper location on the liquid–vapor interface and the neighboring asperity. This assumption was already defended by Extrand, in 2002, in the case of ideally cylindrical asperities [22], as reproduced in Fig. 5[a]. According to Extrand, and to quote from ref. [22]: 'If liquid is injected into the drop, its leading edge will bulge forward, contacting a neighboring asperity'. This assumption has later been experimentally demonstrated by Schellenberger *et al.* in confocal laser-scanning microscopy experiments on surfaces constituted of cylindrical pillars [35], where it can be seen, on the snapshots of their experiment, reproduced in Fig. 5[c], that the drop does advance by contacting the neighboring asperity at an upper location along the liquid–vapor interface. Again, to quote from Schellenberger *et al.*: 'When imaging the advancing front in the induction period with the confocal microscope, we observe that the contact line does not jump from one pillar to the next. Rather, sections of the liquid–vapor interface descend onto the top face of the next micropillar' [35]. We wish to emphasize that, physically, this is the only mechanism that can cause the triple line to advance: indeed, it cannot be a "nonequilibrium jump" (*i. e.* a transient scan) motion between two asperities (such as defined by Huh and Mason: see Fig. 3 of ref. [36]) as the latter only happens in a Wenzel state and would be therefore related to a potential local collapse of the composite-wetting state. As a consequence, we agree with the authors and wish to generalize these observations to more complex surfaces. For that contact to be established in a composite-wetting state, the apparent contact angle (with respect to the horizontal) at the topographical scale n must increase. Nevertheless, as the local contact angle formed by the triple line is already the local advancing contact angle $\theta_{A,n-1}$, the only way it can happen is that the triple line actually undergoes an advancing motion at the topographical scale $n-1$, subsequently increasing the anchorage depth at the topographical scale n, reaching for a location associated with a higher instantaneous slope ω_n. This motion – that we define as a *precursor* advancing motion (that is, a local motion precursor to the advancing motion at a higher scale, similar to that described by Huh and Mason for surfaces wetted in a Wenzel state, as described by the motion between points A' and A'' in Fig. 1 of ref. [36]) – requires the triple line to progress across the rows of asperities constituting the topographical scale $n-1$. Therefore, this induces a recursion relation between all topographical scales: indeed, for the macroscopic lateral motion of the droplet to occur, the triple line has to undergo local motions from the topographical scale $i = 0$ to the scale $i = n$. To illustrate, Fig. 4[a] schematically depicts the mechanism underlying the advancing motion of the triple line at the topographical scale n. The latter occurs

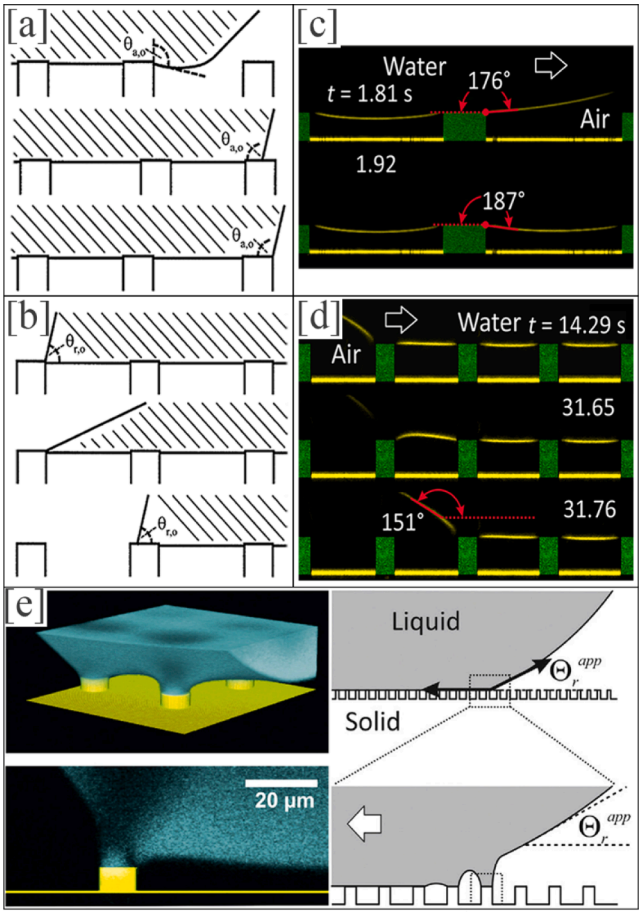

Fig. 5. [a][b] Schematic representations of the mechanisms which drive the advancing ([a]) and the receding ([b]) motions of the triple line: reproduced with permission from ref. [22]; [c][d] Laser-scanning confocal-microscopy images of the front of a droplet undergoing an advancing motion ([c]) and the rear of a droplet submitted to a receding motion ([d]): reproduced with permission from ref. [35]; [e] Laser-scanning confocal-microscopy images of the external baseline of an evaporating droplet and schematic representation of the shape of the liquid–vapor interface: reproduced with permission from ref. [23].

between times t_7 and t_8, but is only possible because a precursor advancing motion occurs at the topographical scale n between times t_3 to t_7 (indeed, between times t_1 to t_3, the local contact angle increases towards $\theta_{A,n-1}$ but the local apparent instantaneous slope remains constant). That precursor advancing motion is due to a local advancing motion occurring at the topographical scale $n-1$ starting at time t_3 after that a precursor advancing motion had been produced at this scale between times t_1 to t_3, itself due to the local advancing motion that started at the topographical scale $n-2$ at time t_1, and so on….

Let us now get back to the moment at which the contact occurs between the liquid–vapor interface and the neighboring asperity at the topographical scale n. By simple geometrical considerations, it is clear that the value of the *advancing anchorage depth*, $d^A_{a,i}$ (see Fig. 1[g], Fig. 4[a] or Fig. 6), at which the triple line is located when the liquid–vapor interface enters into contact with the neighboring asperity, is always smaller than the equilibrium anchorage depth, $d^*_{a,i}$. To predict the value of $d^A_{a,i}$, we shall consider two approximations. First of all, the curvature of the liquid–vapor interface is very small with regards to the dimension of the drop and the radius of curvature of the top of an asperity is small. Therefore, the liquid–vapor interface can be considered flat before the contact occurs and the location of the contact is assumed to be nearly coincident with the top of the neighboring asperity. Second of all, let us consider that, at equilibrium, the meniscus is virtually horizontal. Indeed, we have shown in a previous work that the equilibrium anchorage depth was almost equal to the depth at which the local curvature vanishes [21]. Under these approximations, we can derive the following relation:

$$d^A_{a,i} = d^*_{a,i} - \frac{b_i\left(d^A_{a,i}\right) - b_i\left(d^*_{a,i}\right)}{\tan\left(\theta_{A,i-1} - \frac{\pi}{2}\right)} \tag{5}$$

The exact prediction of $d^A_{a,i}$ remains difficult (Eq. (5) contains two unknowns in spite of previous approximations) since the latter depends on the profiles of spacing and instantaneous slope. Nevertheless, Eq. (5) demonstrates, interestingly, that for values of $\theta_{A,i-1}$ close to π, $d^*_{a,i} - d^A_{a,i}$ tends to vanish. Therefore, $d^A_{a,i}$ depends on the value of $\theta_{A,i-1}$, and, consequently, on the value of $d^*_{a,i}$ (as said before, $d^A_{a,i}$ is always bounded by $d^*_{a,i}$). In fact, the higher the local advancing contact angle, $\theta_{A,i-1}$, the lower $d^A_{a,i}$, and, therefore, the higher the apparent advancing contact angle at the scale i. In addition, the closer the rows of asperities, the smaller $d^A_{a,i}$ and the smaller the apparent advancing contact angle at the scale i. As a result, to render the advancing motion more superficial and increase the apparent advancing contact angle, one must increase the local advancing contact angle and increase the spacing between asperities.

2.3. On the mechanism of the receding motion of triple lines on a multiscale surface

Now, let us treat the case of the receding motion of the triple lines, caused by a continuous reduction of the volume of the drop. Fig. 4[b] schematically depicts a portion of a triple line submitted to a receding motion on the same surface as previously considered. In order for the triple line to undock from one row of asperities, the menisci initially produced between the last row of asperities and the neighboring row must detach. Two mechanisms are involved in this step. First, a precursor receding motion of the triple line happens, which results from local receding motions at all topographical subscales, allowing the external triple line to move towards the anchor point of the meniscus (which corresponds to the motion of the *external liquid front*, as illustrated in Fig. 4[b] at the topographical scale $n-2$). Secondly, the meniscus is actually submitted to a change in its equilibrium curvature due to a locally decreasing bulk pressure caused by the local curvature of the droplet being lowered. Indeed, as the macroscopic contact angle is transiting from its equilibrium value to the macroscopic receding contact angle, the local curvature decreases or even (but not necessarily) switches from a concave to a convex geometry (which would mean a local bulk pressure lower than that of the vapor phase around the drop). The latter phenomenon can be due to evaporation, withdrawal of liquid or to the upstream–downstream motion of the fluid in the case of a tilting plate experiment, which in all cases induces a local depressurization. This causes the anchorage depth of the meniscus to be lowered as another precursor receding motion occurs at the location of the anchor point of the meniscus (which corresponds to the motion of the *meniscus interface*, as identified in Fig. 4[b] at the topographical scale $n-2$). As the two liquid–vapor interfaces draw closer together, those two precursor receding motions cause the triple line to locally 'pinch off and rupture' (similarly to how it has been described by Extrand [22], as reproduced in Fig. 5[b]) at a *receding anchorage depth* $d^R_{a,i}$, which is, subsequently, always smaller than the equilibrium anchorage depth, $d^*_{a,i}$. As a matter of fact, Extrand described, in 2002, a similar mechanism [22], although it was limited in terms of complexity since the surfaces he considered displayed ideally cylindrical asperities, as reproduced in Fig. 5[b]. To quote from ref. [22]: 'The apparent receding contact angle decreases as the contact line tries to establish its "true" receding angle on the side of the asperity. In doing so, the contact line is pinched off and

ruptures. The receding contact line jumps to the next asperity, and the process starts again'. This phenomenon is demonstrated from the laser-scanning confocal-microscopy images published by Schellenberger *et al.*, as reproduced in Fig. 5[d], for the receding motion of a droplet moving on the substrate [35], and from those published by Butt *et al.*, as reproduced in Fig. 5[e], for the receding motion of an evaporating droplet [23]: it can be seen in both scenarios that the meniscus produced between the external row of asperities and the neighboring row is submitted to a change in its curvature due to a lower bulk pressure, allowing the triple line to pinch off. Again, in both works, the conclusions are limited due to the study of cylindrical asperities, and therefore, authors did not describe the two-sided mechanism that we describe herein. To quote from Schellenberg *et al.*: 'The contact line is pinned until a certain lower contact angle is reached. Then the liquid front jumps to the next pillar' [35]. And to quote from Butt *et al.*: 'Capillary bridges are formed between the top faces of the pillars and the drop. […] At the edge, these bridges form neck-like structures. The total curvature in these liquid necks is low because the Laplace pressure of the liquid is determined by the macroscopic radius of the drop. […] For a drop to recede or roll the capillary bridges at the rear have to be broken. […] The liquid bridge collapses when the actual microscopic contact angle decreases below the receding contact angle' [23].

Interestingly, this receding mechanism could even be suspected to leave a small amount of water behind (that is, on the row of asperities that has just been dewetted), as the capillary bridge that is formed between the last two rows of asperities potentially pinches off at a certain distance from the anchor point (as represented in Fig. 4[b], at the topographical scale $n-2$ at time t_3), which would confirm what has been suggested by Patankar [37], Roura and Fort [38] and Choi *et al.* [39] (see fig. S4 of Ref. [39]). Eventually, these qualitative considerations allow us to draw the conclusion that the receding motion of the triple line at the topographical scale i is driven by the local receding contact angle at the scale $i-1$, $\theta_{R,i-1}$, by the profile of the instantaneous slope, $\omega_i(d_{a,i})$, and, interestingly, by the equilibrium anchorage depth (which itself depends on the local advancing contact angle at the scale $i-1$), $d^*_{a,i}(\theta_{A,i-1})$.

2.4. From the description of the advancing and receding motions to the prediction of the contact angle hysteresis

Before jumping into the prediction of the CAH, it must be said that both the advancing and receding mechanisms are subsequently intrinsically discontinuous. The advancing and receding motions can therefore occur in a microscopic stick–slip fashion. If experimental observations often show these motions as *apparently* continuous, it is due to the lack of magnification and resolution inherent to the optical systems that are commonly used. However, macroscopic stick–slip motions are sometimes witnessed, such as what has been reported and theoretically analyzed by Shanahan [40]. To understand these macroscopic stick–slip motions, one need to transpose what Huh and Mason suggested when studying surfaces wetted in a Wenzel state to a composite-wetting state. Based on their conclusions, we can suggest that while the inertia of the triple line enables it to advance or recede over macroscopic distances, macroscopic stick–slip motions could result from the competition between inertia and viscous dissipation due to the propagation of a perturbation wave along the liquid–vapor interface when the latter is deformed as the triple line contacts (when advancing) or pinches off (when receding). The liquid–vapor interface subsequently displays transient nonequilibrium shapes, such as depicted in Fig. 4[a] and 4[b], producing said perturbation wave as the liquid–vapor interface tries to minimize its area accordingly to thermodynamical considerations. These discontinuous motions are demonstrated by the results introduced by Schellenberger *et al.* [35], as reproduced in Fig. 5[c] and 5[d], and by Butt *et al.* [23], as reproduced in Fig. 5[e]. As a final note, based on our previous theoretical considerations, the theoretical results obtained by Huh and Mason [36] and Shanahan [40] and the experimental observations of Schellenberger *et al.* [35] and Butt *et al.* [23], we can claim that the advancing and receding motions are discontinuous attempts of the droplet to return towards a global energy minimum by, respectively, reducing and increasing the macroscopic contact angle formed by the latter with the surface in response to an external source of free energy.

Eventually, based on these considerations and on the expressions relating apparent angles to fractional contributions that were suggested by Extrand [22], we can introduce the following recursion relations:

$$\theta_{A,i} = \lambda_i\left(d^A_{a,i}\right)\left[\theta_{A,i-1} + \omega_i\left(d^A_{a,i}\right)\right] + \left(1-\lambda_i\left(d^A_{a,i}\right)\right)\pi \tag{6}$$

$$\theta_{R,i} = \lambda_i\left(d^R_{a,i}\right)\left[\theta_{R,i-1} - \omega_i\left(d^R_{a,i}\right)\right] + \left(1-\lambda_i\left(d^R_{a,i}\right)\right)\pi \tag{7}$$

where, noticeably:

(1) $d^A_{a,i} < d^*_{a,i}$ with $d^A_{a,i}$ depending on the profile of the instantaneous slope, on the profile of the spacing between two asperities and on the equilibrium anchorage depth, $d^*_{a,i}$, which itself depends on the local advancing contact angle at the topographical scale $i-1$, $\theta_{A,i-1}$;
(2) $d^R_{a,i} < d^*_{a,i}$ with $d^R_{a,i}$ depending on the profile of the instantaneous slope, on the local receding contact angle at the topographical scale $i-1$, $\theta_{R,i-1}$, and on the equilibrium anchorage depth, $d^*_{a,i}$, which itself depends on the local advancing contact angle at the topographical scale $i-1$, $\theta_{A,i-1}$;
(3) λ_i is the profile of external triple-line density (apparent at the scale i) as a function of the anchorage depth, $d_{a,i}$ (and is monotonically increasing with the latter when the asperities are non-reentrant, that is, such that, for all $d_{a,i} \geq 0, \omega_i(d_{a,i}) < \frac{\pi}{2}$).

Therefore, the contact angle hysteresis at the topographical scale i, $\Delta\theta_i$, can be expressed as:

$$\begin{aligned}\Delta\theta_i = {} & \lambda_i\left(d^A_{a,i}(\theta_{A,i-1})\right)\left[\theta_{A,i-1} + \omega_i\left(d^A_{a,i}\right) - \pi\right] \\ & - \lambda_i\left(d^R_{a,i}(\theta_{A,i-1})\right)\left[\theta_{R,i-1} - \omega_i\left(d^R_{a,i}\right) - \pi\right]\end{aligned} \tag{8}$$

It is noteworthy that, in Eqs. (6) and (7), the advancing (respectively, the receding) contact angle, $\theta_{A,i}$ (resp. $\theta_{R,i}$), is calculated from the sum of $\theta_{A,i-1} + \omega_i\left(d^A_{a,i}\right)$ (resp. $\theta_{R,i-1} - \omega_i\left(d^R_{a,i}\right)$) and π weighted by the fractional contributions λ_i and $(1-\lambda_i)$. We deliberately did not use cosines as in the Cassie-Baxter model or the modified Cassie-Baxter model introduced by Choi *et al.* [39]. Indeed, the Cassie-Baxter model is based on an energetical approach where the work of adhesion is averaged along the triple line (in reality, authors study a neighboring area around the triple line, meaning that they resort to an area approach). Here, we wish to resort to a geometrical approach (or a triple line approach) where it is considered that the triple line is the only location where the contact angle hysteresis is determined, in line with previous works [41–43]. Therefore, we agree with Extrand that the advancing and receding contact angles '*manifest themselves as fractional contributions along the contact line*' (to quote from Ref. [22]). These considerations are supported by experimental evidence [44–45].

3. Discussion

3.1. A new criterion for contact angle hysteresis

In the case of a surface constituted of n topographical scales, values of $\theta_{A,n}$ and $\theta_{R,n}$ respectively given by Eqs. (6) and (7) might significantly vary from those measured through the use of an optical goniometer. For surfaces with a large spacing between protrusions and with superficial penetration of water between the latter, Eq. (6) yields angles close to π.

In fact, Schellenberger *et al.* have shown, through laser-scanning confocal microscopy experiments realized on a surface constituted of micrometric pillars, that the advancing contact angle happened to oscillate between 170° and 185° when an apparent advancing contact angle of 165° was measured with conventional optical goniometry [35]. We, therefore, agree with Schellenberger *et al.* on the need to revisit the criterion on the value of the contact angle hysteresis usually considered in the definition of a superhydrophobic surface ($\Delta\theta = \theta_A - \theta_R < 10^{\circ}$). Indeed, this criterion depends on the method used to measure the advancing and receding contact angles. We believe that, when these angles have values close to or above 150° (as typically observed on textured surfaces submitted to a composite-wetting state), another criterion, based exclusively on the value of the receding contact angle, should be considered. Schellenberger *et al.* have suggested defining a superhydrophobic surface by an apparent receding contact angle equal to or exceeding 150°, suggestion with which we agree.

3.2. On the dependence of equilibrium anchorage depths on topographical subscales

With the aim of deriving a general recursion relation between the above-mentioned parameters and the equilibrium anchorage depth displayed at the topographical scale $i = n$, we shall now consider a hierarchical surface constituted of n topographical scales, as depicted in Fig. 3[b] (view at scale n) and 3[c] (close-up view at scale $n-1$).

In Eq. (4), the solutions to $\Delta P_i(d_{a,i}) = 0$ and $z_{f,i}(d_{a,i}) > 0$ exclusively depend on the profile $\omega_i(d_{a,i})$, the profile $b_i(d_{a,i})$ and the local advancing contact angle $\theta_{A,i-1}$. In other terms, and most interestingly, for all n, the equilibrium anchorage depth at the topographical scale n can be predicted if one knows the profiles $\omega_n(d_{a,n})$ and $b_n(d_{a,n})$ (which can be determined experimentally through optical profilometry, tilted observations under a secondary electron microscope or atomic force microscopy) and the local advancing contact angle $\theta_{A,n-1}$ (which can be determined experimentally through the reproduction of a surface constituted of topographical subscales i from 0 to $n-1$, such as what has been done by Bhushan *et al.* [46] and Koch *et al.* [47], who performed recrystallization experiments of extracted epicuticular wax to replicate the sacred lotus nanotubules on flat substrates, enabling the measurement of $\theta_{A,n-1}$). This seems to be the least complex path towards the prediction of equilibrium anchorage depths on multiscale surfaces at a given topographical scale – such as what has been done in previous works [20–21] – and towards understanding the link between equilibrium anchorage depths and the CAH at the topographical scale n (which can be measured – if the latter is the scale of largest order of magnitude – by measuring the macroscopic CAH). The other alternative is much more complex as it requires to calculate every input parameter relative to the topography, to know the intrinsic advancing contact angle $\theta_{A,0}$ (the latter being accessible experimentally, as described in previous works [20–21]) and to calculate all the local advancing contact angles proper to intermediate topographical scales through Eq. (6). Note that in all cases, no knowledge of the solid–liquid or solid–vapor interfacial tensions is required, since this information is already contained in the local advancing contact angle $\theta_{A,0}$, and, thus, by the recursion relation introduced in Eq. (6), in all the local advancing contact angles, $\theta_{A,i}$, for all i from 0 to n, given the knowledge of all topographical parameters.

3.3. On the link between the equilibrium anchorage depth and the contact angle hysteresis

We wish to emphasize here that the modeling introduced in this paper allows to better understand the link between the degree of penetration of water between protrusions and the CAH of a surface. Indeed, as we have shown, the mechanisms underlying the advancing and receding motions of the triple line depend on the location of the meniscus at equilibrium, since both $d^A_{a,i}$ and $d^R_{a,i}$ are bounded by the equilibrium anchorage depth, $d^*_{a,i}$. Therefore, minimizing the latter eventually comes to reducing the values of $\lambda_i\left(d^A_{a,i}\right)$ and $\lambda_i\left(d^R_{a,i}\right)$, and, therefore, lowering the amplitude of the CAH. As a conclusion, our theoretical considerations explain the adhesive behavior of surfaces producing a large equilibrium anchorage depth or even associated with a rose-petal wetting state: surfaces displaying a large equilibrium anchorage depth actually display a high advancing contact angle and a low receding contact angle only because they are characterized by large values of advancing and receding anchorage depths. Since the two latter are bounded by the equilibrium anchorage depth, one should target a low equilibrium anchorage depth at the topographical scale of largest order of magnitude in order to obtain a reduced adhesion.

3.4. On the effect of a topographical subscale on water-repellency

In the spirit of describing whether or not adding a topographical scale i via a more sophisticated manufacturing process is worth it regarding its effect on the macroscopic CAH, one must draw up a comparison between the case where that topographical scale does exist and the case where not. In other terms, the relevance of a topographical scale i lies, for a surface constituted of n topographical scales, in its effect on the value of $\Delta\theta_n = \theta_{A,n} - \theta_{R,n}$ in comparison with a reference value predicted without it, $\Delta^{ref}\theta_n = \theta^{ref}_{A,n} - \theta^{ref}_{R,n}$, that is, with a flat layer constituting the topographical scale under study ($\theta^{ref}_{A,i} = \theta_{A,i-1}$ and $\theta^{ref}_{R,i} = \theta_{R,i-1}$). In order to clearly illustrate this approach, let us treat the simple case of a surface constituted of two topographical scales (typically, a vegetal surface constituted of protuberant micrometric cells covered with nanoscale epicuticular wax crystals or an industrial surface produced by femtosecond laser manufacturing where the scale $i = 2$ is due to the ablation process and can be a square network of micrometric pillars and the scale $i = 1$ corresponds to nanoscale ripples resulting from the light-matter interactions). The relevancy of adding the topographical subscale $i = 1$ is given according to the sign of $\Delta\theta_2 - \Delta^{ref}\theta_2$. In the latter expression, $\Delta\theta_2$ is calculated from Eq. (8) by inputting $\theta_{A,1}$ and $\theta_{R,1}$, when $\Delta^{ref}\theta_2$ is similarly calculated by inputting $\theta_{A,0}$ and $\theta_{R,0}$ instead. It yields an important conclusion regarding the consequence of an enhanced surface topography through the texturing of the topographical subscale i $= 1$. Adding a topographical scale always lead to an increase of the local advancing contact angle since it comes to enhancing the mechanical pinning of the triple line at the advancing contact angle [20–21,35,48]. Thus, let us suppose $\theta_{A,1} > \theta_{A,0}$. As described in previous works [20–21], the increase of $\theta_{A,1}$ leads to a lower equilibrium anchorage depth, and, subsequently, to lower external-contact-line linear density (since $\lambda_2(d_{a,2})$ monotonically decreases with $d_{a,2}$, and given the fact that both $d^A_{a,2}$ and $d^R_{a,2}$ are bounded by $d^*_{a,2}$). Therefore, even in the case where this additional topographical subscale is wet in a Wenzel state, if the effect of the increase of the local advancing contact angle $\theta_{A,1}$ on the equilibrium anchorage depth is such that the decrease of $\lambda_2\left(d^A_{a,2}\right)$ and $\lambda_2\left(d^R_{a,2}\right)$ overcomes a potential decrease of the local receding contact angle, adding another topographical subscale might be beneficial (*i. e.* $\theta_{A,2} - \theta_{R,2}$ could decrease). Now, the propagation of this effect is guaranteed, since *at constant chemistry*, for all i, $\theta_{A,i+1} > \theta_{A,i}$. Therefore this potential beneficial effect can be propagated, by immediate recursion, to the case of a surface constituted of n topographical scales. In other terms, a topographical scale i wetted in a Wenzel state might still be relevant with regards to the macroscopic CAH due to the competition between a lower equilibrium anchorage depth at the topographical scale $i+1$ and a higher contact angle hysteresis at the topographical subscale i. In a forthcoming article, we experimentally illustrate these claims.

3.5. On the effect of a topographical subscale on the robustness of the composite-wetting state

In the continuation of the last considerations, the relevance of adding a given topographical subscale must also be considered as for its effect on the stability of the composite-wetting state at scales of larger orders of magnitude. As a matter of fact, as emphasized in a previous paper within the framework of a practical example [21], the maximal overpressure, $\Delta P_{max,i}$, that can be sustained before a transition between a composite-wetting state to a Wenzel state at a given topographical scale i, and the reference maximal overpressure, $\Delta^{ref}P_{max,i}$, obtained for a topographical subscale $i-1$ that would be flat (*i.e.* $\theta^{ref}_{A,i-1} = \theta_{A,i-2}$) are given by the expressions:

$$\Delta P_{max,i} = \gamma \frac{-\sin\left(\omega_i^{max} + \theta_{A,i-1}\right)}{b_i\left(d^m_{a,i}\right)} - \gamma C_{macro} - \rho g \Delta z \tag{11}$$

$$\Delta^{ref} P_{max,i} = \gamma \frac{-\sin\left(\omega_i^{max} + \theta_{A,i-2}\right)}{b_i\left(d^m_{a,i}\right)} - \gamma C_{macro} - \rho g \Delta z \tag{12}$$

In the latter, ω_i^{max} is the maximal instantaneous slope, reached at an anchorage depth $d^m_{a,i}$. Therefore, the topographical subscale $i-1$ is relevant as for the robustness of the composite-wetting state at the scale i if and only if $\Delta P_{max,i} > \Delta^{ref}P_{max,i}$, which directly yields $\theta_{A,i-1} > \theta_{A,i-2}$. Since a non-flat topography will always promote a higher local advancing contact angle in comparison with a flat local surface [20–21,48],$\theta_{A,i-1}$ is always higher than $\theta_{A,i-2}$. Thus, these considerations lead to an important result: adding an additional topographical subscale always increases the robustness of the composite-wetting state (at constant chemistry). Here, an immediate recursion yields the conclusion that, for all j from 2 to n, if for all i from 2 to j, $\theta_{A,i-1} > \theta_{A,i-2}$, then, $\Delta P_{max,j} > \Delta^{ref}P_{max,j}$. Therefore, the positive effect of adding a topographical subscale $i-1$ is propagated to the robustness proper to all topographical scales of larger orders of magnitude.

This important result is consistent with our recent findings, as published elsewhere [21]: we have demonstrated, by using Eq. (11) and applying it to the chemistry and the topography of the sacred lotus (*Nelumbo nucifera*) leaf, that the adaxial side of the latter is constituted of a two-scale hierarchical surface topography that produces a composite-wetting state capable of withstanding overpressures up to approximately $10kPa$ thanks to its nanoscale topography. Without a nanoscale topography, this maximal overpressure is lowered. Therefore, adding a nanoscale topography is a key ingredient in the lotus leaf's recipe for a robust Cassie-Baxter state at the micrometric scale. A notable result is that this order of magnitude of overpressures corresponds to that caused by the impacts of droplets in a heavy rain, meaning that *Nelumbo nucifera* has evolved to endure the harshest conditions in its environment without being over-dimensioned. The additional mechanical pinning exerted by the nanoscale topography on the advancing sections of the triple line is paramount to the robustness of its composite-wetting state since it increases the value of the local advancing contact angle and, thus, the value of the maximal sustainable overpressure. In the end, its nanoscale topography enables it to reduce the density of papilla per unit of area (and, subsequently, to increase its water-repellency and to decrease the energy cost associated with the formation of new leaves and their growth) while enhancing its robustness.

3.6. On changing the liquid, the external conditions or adding a curvature

The modeling described herein also allows to discuss the effect of other parameters on the equilibrium conditions and the CAH, such as the nature of the liquid, the temperature or the humidity of the environment surrounding the drop.

Pure water has the highest liquid–vapor interfacial tension among liquids – leaving aside liquid metals such as mercury. When using other liquids characterized by a lower surface tension, not only γ decreases, but so does every contact angle characterizing the solid–liquid system, including the intrinsic advancing contact angle. This means that, at the smallest topographical scale, the equilibrium will be found at a deeper location or will not be found at all if the liquid surface tension is too low. As a consequence, the advancing contact angle formed at the smallest topographical scale will be lowered, as deduced from Fig. 6. By recursion relation, every local advancing contact angle at topographical scales of larger orders of magnitude will be lowered and the system will tend towards a drop anchored more deeply at the topographical scale of the highest order of magnitude. Therefore, it will display a higher macroscopic CAH. This can even cause the drop to be anchored in a Wenzel state at its highest topographical scale and, therefore, to the production of a rose-petal effect. When using oils, which are characterized by a very low surface tension, it will be more challenging in terms of surface morphology to produce an air-entrapment state. Indeed, oils tend to form intrinsic advancing contact angles that are hydrophilic. Therefore, it will require a reentrant morphology at the smallest topographical scale to keep an air-entrapment state leading to a hydrophobic local advancing contact angle at the smallest topographical scale and subsequently at larger topographical scales as well. When using raindrops or water in which a certain quantity of surfactants is dissolved, it is known that the surface tension of water is subsequently lowered [49]. Therefore, the same considerations as described above are applied in the case of impure water or an aqueous solution that includes surfactants.

In a similar manner, when the temperature increases in the environment surrounding the drop, the surface tension of the liquid

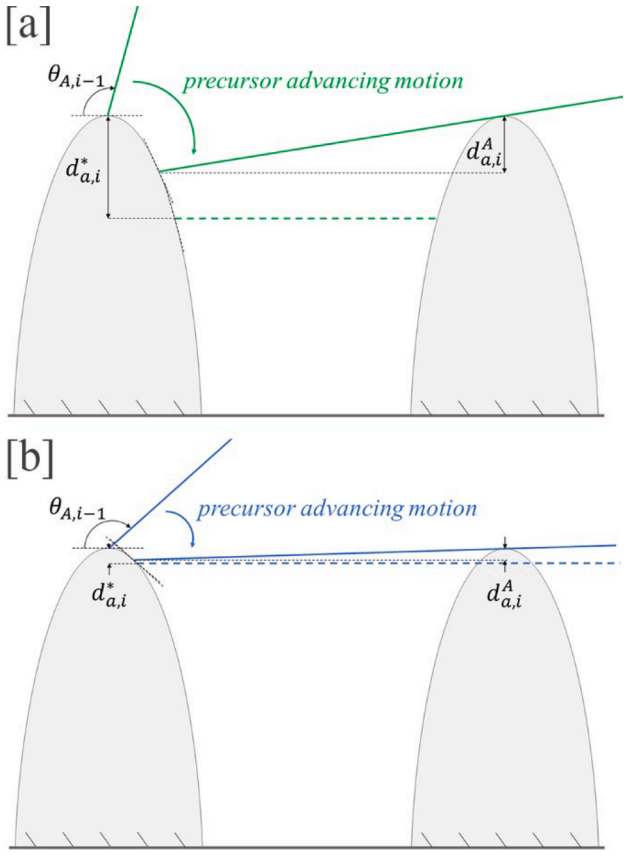

Fig. 6. Schematical representation of the geometrical conditions at which the advancing motion is initiated at the topographical scale i: [a] with a low local advancing contact angle; [b] with a high local advancing contact angle. In dashed lines, a flat meniscus is represented at the equilibrium anchorage depth (under the hypothesis where no overpressure is applied on the drop).

decreases because the cohesion forces within the liquid phase are weaker [49]. The same evolution is noticed as the humidity in the air surrounding the drop increases: the steam acts as a surfactant for the liquid–vapor interface and the liquid–vapor interfacial tension decreases [50].

When tilting the sample, one could question the effect of the direction of gravitational forces. As previously demonstrated [21], the effect of gravity is negligible for the local equilibrium. Therefore, inclined surfaces will not have an effect on the values of equilibrium, advancing and receding anchorage depths, and therefore on the value of the CAH. Nevertheless, if the role of gravity is negligible regarding the local equilibrium, it obviously plays a key role at the macroscopic scale as it allows to undock the drop when the surface is water-repellent. It is the source of the free energy given to the drop as it locally deforms to display its advancing and receding contact angles.

Eventually, a surface can also display a curvature. In such cases, one has to question what is the scale of the curvature. If it is much larger that the size of the droplet, it will not have an effect on the equilibrium and on the CAH. If it much smaller that the size of the droplet, it will constitute in itself a topographical scale and will be studied as such as described in our model. Inbetween, its effect can be included as a modification to the profile of local slope of the largest topographical scale.

3.7. On the independence of topographical subscales

As a final note, we shall emphasize that in all the discussions above, we have considered the effect of the local advancing contact angle produced at a topographical subscale i on the curvature of the menisci anchored at the topographical scale $i+1$. For these considerations to remain valid, all topographical scales must be independent from the others. In other terms, and more practically, for all i, the characteristic length of the asperities constituting the scale $i+1$ must be very large when compared to that associated with the topographical subscale i.

4. Conclusions

In this theoretical study, we intend to shed light on the way real multiscale surfaces interact with a liquid droplet. At equilibrium, during the advancing motion or during the receding motion, the behavior of triple lines and menisci is thoroughly investigated and, for the first time, recursion relations between each topographical scale that constitutes a surface are described. We introduce important new definitions that bridge a paramount conceptual gap for the description of wetting on multiscale surfaces that display non-model topographies such as in nature. Then, we carry out an analytical modeling of wetting that yields important conclusions regarding the effect of additional topographical scales on the stability of the air-entrapment state as well as the link between the degree of penetration of water and the so-called 'rose-petal effect'. These conclusions are summarized as follows:

(1) We formally introduce the concept of *equilibrium anchorage depth*, in continuation with our previous works realized on the lotus leaf [20–21], as the location where menisci are anchored on the side of surface asperities when the droplet is at equilibrium in an air-entrapment state. This value is proper to each topographical scale. We prove that the equilibrium anchorage depth at the topographical scale i only depends on the topographical signature proper to the scale i (more practically, the profiles of the local slope and of the spacing between two anchor points) and on the local advancing contact angle at the scale $i-1$, which supposes that all topographical scales are recursively linked together;
(2) Based on a series of conceptual and experimental works published in the past decades, such as the pioneer works of Extrand [22], Schellenberger *et al.* [35] and Butt *et al.* [23], we adapt the study to the case of a non-model multiscale surface and we thoroughly describe the mechanisms which drive the attachment/detachment of the menisci during the advancing or the receding motion of the external triple lines of a droplet. The advancing motion occurs as the liquid–vapor interface contacts the next row of asperities and is therefore intrinsically discontinuous. The receding motion occurs as the result of two motions of the liquid–vapor interface, one that is external, the other that comes from the rise of the meniscus due to a local transient pressure depletion, subsequently causing the liquid–vapor interface to pinch off and rupture, leaving a small quantity of liquid behind, which resolves some questions raised by previous authors [37–39];
(3) We define, for the first time, the notions of *precursor advancing motion* and *precursor receding motion*, which precede an advancing or a receding motion at a given topographical scale: they consist in a local motion, over a small distance with regards to the considered scale, due to an advancing or a receding motion occurring at a smaller topographical scale, which induces a recursion relation between all topographical scales. In other terms, the advancing or the receding motions are propagated along all topographical scales before they can occur macroscopically. We hereby bridge an important conceptual gap for the study of composite-wetting state occurring on multiscale surfaces, in continuation of the pioneer work of Huh and Mason for mono-scale surfaces wetted in a Wenzel state [36];
(4) We introduce new parameters, namely the *advancing anchorage depth* and the *receding anchorage depth*, which locates the pinning points of the menisci at the very moment when the latter contacts the next row of asperities and detaches from the last row of asperities, respectively. We derive how the CAH at a given topographical scale is related to those two parameters, opening the way for the prediction of its value on complex surfaces. The more the spacing, the less the CAH. The more the local advancing contact angle, the less the CAH. The more the local slope, the less the CAH;
(5) We demonstrate how the monitoring of the equilibrium anchorage depth can be sufficient to lower the CAH: the equilibrium anchorage depth is always an upper bound for the values of the advancing and receding anchorage depths. As a consequence, the less the equilibrium anchorage depth, the less the CAH. Therefore, we shed light on how the penetration of liquid between asperities is associated to the 'rose-petal effect', contributing to filling the lack of physical insights about this phenomenon that has been at the center of a lot of focus in the past decades [18–19,51];
(6) Eventually, we formally demonstrate that an additional topographical subscale always increases the robustness of the air-entrapment state as it contributes to the stability of the anchorage of the menisci submitted to an external overpressure. In line with this conclusion, we reaffirm the need for designing efficient multiscale manufacturing processes to achieve water-repellent surfaces offering reliable behaviors over a wide range of external overpressures and that are, therefore, suitable within a broad spectrum of technological applications, in line with our previous study [21].

CRediT authorship contribution statement

Yann Bami Chatenet: Writing – review & editing, Writing – original draft, Visualization, Validation, Methodology, Investigation, Formal analysis, Conceptualization. **Stéphane Valette:** Writing – review & editing, Visualization, Supervision, Resources, Project administration, Funding acquisition.

Declaration of competing interest

The authors declare that they have no known competing financial interests or personal relationships that could have appeared to influence the work reported in this paper.

Data availability

Data will be made available on request.

Acknowledgement

This work was supported by the French Ministry of Higher Education and Research.

The authors wish to gratefully acknowledge the help provided by Jean-François Thomas, David Scherberich and the botanical garden of Lyon as they provided samples of sacred lotus leaves.

References

[1] W. Barthlott, C. Neinhuis, Planta. 202 (1997) 1–8.
[2] S. Herminghaus, Europhys. Lett. 52 (2000) 165–170.
[3] M. Nosonovsky, B. Bhushan, Microelectron. Eng. 84 (2007) 382–386.
[4] Y. Kwon, N. Patankar, J. Choi, J. Lee, Langmuir. 25 (2009) 6129–6136.
[5] G. Whyman, E. Bormashenko, Langmuir. 27 (2011) 8171–8176.
[6] A. Marmur, S. Kojevnikova, J. Colloid Interface Sci. 568 (2020) 148–154.
[7] A.B.D. Cassie, S. Baxter, Trans. Faraday Soc. 40 (1944) 546–551.
[8] C.G.L. Furmidge, J. Colloid Sci. 17 (1962) 309–324.
[9] D.C. Pease, J. Phys. Chem. 49 (1945) 107–110.
[10] J.F. Joanny, P.G. de Gennes, J. Chem. Phys. 81 (1984) 552–562.
[11] H.-J. Butt, et al., Curr. Opin. Colloid Interface Sci. 59 (2022) 101574.
[12] K. R. M, S. Misra, S.K. Mitra, Langmuir. 36 (2020) 13689–13697.
[13] S. Shyam, S. Misra, S.K. Mitra, J. Colloid Interface Sci. 630 (2023) 322–333.
[14] Y. Sun, et al., Surf. Innov. 6 (2018) 93–105.
[15] J.W. Drelich, Adv. Colloid Interface Sci. 267 (2019) 1–14.
[16] M. Villegas, Y. Zhang, N. Abu Jarad, L. Soleymani, T.F. Didar, ACS Nano. 13 (2019) 8517–8536.
[17] A. Rajak, J. Rühe, Adv. Mater. Interfaces. 9 (2022) 2201018.
[18] B. Bhushan, M. Nosonovsky, Philos. Trans. Royal Soc. a. 368 (2010) 4713–4728.
[19] S. Choo, H.-J. Choi, H. Lee, Mater. Lett. 121 (2014) 170–173.
[20] Y. Bami Chatenet, S. Valette, Colloids Surf. A: Physicochem. Eng. Asp. 672 (2023) 131752.
[21] Y. Bami Chatenet, S. Valette, Colloids Surf. A: Physicochem. Eng. Asp. 682 (2024) 132877.
[22] C.W. Extrand, Langmuir. 18 (2002) 7991–7999.
[23] H.-J. Butt, D. Vollmer, P. Papadopoulos, Adv. Colloid Interface Sci. 222 (2015) 104–109.
[24] A. Lafuma, D. Quéré, Nature Mater. 2 (2003) 457–460.
[25] B. He, N.A. Patankar, J. Lee, Langmuir. 19 (2003) 4999–5003.
[26] C.W. Extrand, Langmuir. 20 (2004) 5013–5018.
[27] N.A. Patankar, Langmuir. 20 (2004) 7097–7102.
[28] C. Ishino, K. Okumura, D. Quéré, EPL. 68 (2004) 419.
[29] Q.-S. Zheng, Y. Yu, Z.-H. Zhao, Langmuir. 21 (2005) 12207–12212.
[30] E. Bormashenko, Adv. Colloid Interface Sci. 222 (2015) 92–103.
[31] A. Sarkar, A.-M. Kietzig, Soft Matter. 11 (2015) 1998–2007.
[32] C.W. Extrand, Langmuir. 27 (2011) 6920–6925.
[33] C.W. Extrand, S.I. Moon, Langmuir. 30 (2014) 8791–8797.
[34] Y. Jiang, J. Lian, Z. Jiang, Y. Li, C. Wen, Adv. Colloid Interface Sci. 278 (2020) 102136.
[35] F. Schellenberger, N. Encinas, D. Vollmer, H.-J. Butt, Phys. Rev. Lett. 116 (2016) 096101.
[36] C. Huh, S.G. Mason, J. Colloid Interface Sci. 60 (1977) 11–38.
[37] N.A. Patankar, Langmuir. 19 (2003) 1249–1253.
[38] P. Roura, J. Fort, Langmuir. 18 (2002) 566–569.
[39] W. Choi, A. Tuteja, J.M. Mabry, R.E. Cohen, G.H. McKinley, J. Colloid Interface Sci. 339 (2009) 208–216.
[40] M.E.R. Shanahan, Langmuir. 11 (1995) 1041–1043.
[41] F.E. Bartell, J.W. Shepard, J. Phys. Chem. 57 (1953) 455–458.
[42] C.W. Extrand, Langmuir. 19 (2003) 3793–3796.
[43] L. Gao, T.J. McCarthy, Langmuir. 23 (2007) 3762–3765.
[44] C.W. Extrand, Langmuir. 9 (1993) 475–480.
[45] L. O. Brockway, R. L. Jones, in Contact Angle, Wettability, and Adhesion (American Chemical Society, 1964; https://doi.org/10.1021/ba-1964-0043.ch019), vol. 43 of Advances in Chemistry, pp. 275–294.
[46] B. Bhushan, Y.C. Jung, A. Niemietz, K. Koch, Langmuir. 25 (2009) 1659–1666.
[47] K. Koch, B. Bhushan, Y.C. Jung, W. Barthlott, Soft Matter. 5 (2009) 1386–1393.
[48] R.H. Dettre, R.E. Johnson, in Contact angle, wettability, and adhesion (American Chemical Society, 1964; https://doi.org/10.1021/ba-1964-0043.ch008), vol. 43 of Advances in Chemistry, pp. 136–144.
[49] P.-G. de Gennes, F. Brochard-Wyart, D. Quéré, Capillarity and Wetting Phenomena, (Springer, New York, NY, 2004.
[50] J.L. Pérez-Díaz, M.A. Álvarez-Valenzuela, J.C. García-Prada, J. Colloid Interface Sci. 381 (2012) 180–182.
[51] U.U. Ghosh, S. Nair, A. Das, R. Mukherjee, S. DasGupta, Colloids Surf. a: Physicochem. Eng. Asp. 561 (2019) 9–17.